International Journal of Mass Spectrometry 305 (2011) 228–237

Contents lists available at ScienceDirect

International Journal of Mass Spectrometry

journal homepage: www.elsevier.com/locate/ijms

AP-MALDI imaging of neuropeptides in mouse pituitary gland with 5 μm spatial resolution and high mass accuracy

Sabine Guenther[a], Andreas Römpp[a], Wolfgang Kummer[b], Bernhard Spengler[a,*]

[a] Justus Liebig University, Institute of Inorganic and Analytical Chemistry, Giessen, Germany
[b] Justus Liebig University, Institute of Anatomy and Cell Biology, Giessen, Germany

ARTICLE INFO

Article history:
Received 7 August 2010
Received in revised form 26 October 2010
Accepted 8 November 2010
Available online 18 November 2010

Keywords:
MS imaging
Neuropeptide
High spatial resolution
Accurate mass

ABSTRACT

MALDI MS imaging is a powerful tool to visualize the spatial distribution of endogenous biomolecules such as lipids or neuropeptides. Direct identification of analytes is often difficult due to the complexity of biological tissue samples. Today reliable analyte identification is routinely done with mass spectrometers featuring high mass resolving power, high mass accuracy and MS/MS capability. These mass spectrometers, however, typically have a rather poor spatial resolution when used in MALDI MS imaging experiments. In this work a linear ion trap orbital trapping mass spectrometer combined with an in-house developed atmospheric pressure MALDI imaging ion source was used to image neuropeptides in mouse pituitary gland with a spatial resolution of 5 μm.

Ten neuropeptides were identified by their accurate mass in the mass range up to 2500 u via targeted database search. The ion images of the peptides show down to the cellular level that their appearances within the pituitary gland are restricted to accurately defined tissue types. This is in excellent agreement with the gland's structure and biological function.

The identity of the neuropeptides was confirmed by additional MS/MS measurements from single 10 μm sample spots, obtained directly from tissue. Furthermore, MS/MS imaging of two different peptides at 10 μm spatial resolution resulted in product ion images, which were in good accordance with the distributions of their peptide precursor ions, confirming their identity and excluding possible analyte interferences. Since the method offers high performance mass spectrometry in combination with high spatial resolution, it appears to be ideally suited for imaging peptide signatures on a cellular level with high confidence in identification and with high sensitivity.

1. Introduction

Mass spectrometry imaging (MSI) has become a widely used analytical technique due to its ability to visualize the distribution of various analytes in tissue. In contrast to secondary ion mass spectrometry (SIMS), MALDI MSI covers a higher mass range and is able to detect intact biomolecules such as peptides and proteins [1–5]. Neuropeptides are a complex set of messenger molecules controlling a wide array of regulatory functions and behaviors within an organism. They play an important role in many physiological and disease-related processes. Since closely related neuropeptides often contain stretches of identical amino acid sequences, often differ in as little as one single amino acid, and often are post-translationally modified, their simultaneous identification and localization in biological tissue is a challenging task requiring sensitive and versatile mass spectrometers. Previous approaches to identify neuropeptides and localize them in organisms featured high spatial resolution [1,6], high mass resolving power and mass accuracy [7,8] or MS/MS capability [9–11] but not combined in one single experiment. All three of these features, however, are needed to investigate neuropeptides and their function at a cellular level in tissue. A limited sensitivity of high performance mass analyzers for a long time hampered their combination with high spatial resolution analysis, since the number of ions is known to decrease dramatically with a decrease in sampled area. Recently we introduced an instrumental setup which provides high spatial resolution imaging with a mass spectrometer featuring high mass accuracy, high mass resolution and MS/MS capability [12]. Matrix application is another critical point for highly resolved measurements of peptides. For high spatial resolution measurements at the cellular level, matrix application protocols are needed which result in uniform and microcrystalline matrix layers. Matrix crystals have to be smaller than the pixel size in order to prevent analyte migration during analyte incorporation into the matrix crystals upon desolvation. Matrix preparation protocols leading to small matrix crystal sizes have been reported

* Corresponding author.
E-mail address: Bernhard.Spengler@anorg.Chemie.uni-giessen.de (B. Spengler).

1387-3806/$ – see front matter © 2010 Elsevier B.V. All rights reserved.
doi:10.1016/j.ijms.2010.11.011

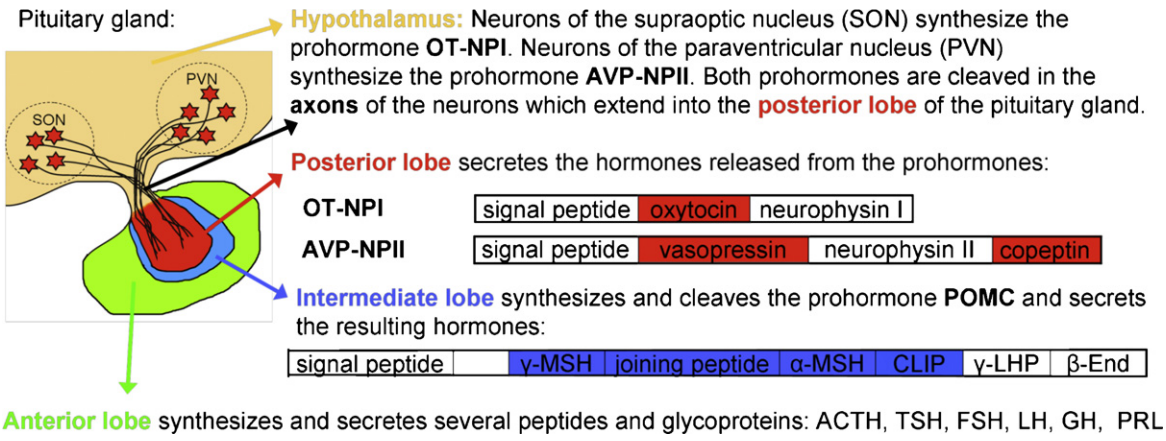

Fig. 1. Structure and biological function of pituitary gland.

[9,13], but they require matrix application in a dry or powder-like manner. These preparation methods work well for the analysis of lipids in biological tissue, but result in a less efficient incorporation of the peptides/proteins into the matrix crystals because of limited wetting of the tissue. We therefore presented a matrix application method for high resolution imaging recently that is applicable to peptides [14].

Mus musculus is a highly investigated mammalian model system with a completely sequenced genome. The hypothalamus and the pituitary gland are the best known neuropeptide secreting organs in mammals. Neuropeptides are formed in vivo by cleavage of proteins at specific cleavage sites and often undergo various posttranslational modifications to activate their biological function.

The pituitary gland is a small-sized oval organ (Fig. 1) [15]. Its typical dimensions in mice are about 3 mm × 1 mm. Its center is formed by the posterior lobe, which is composed of glial cells and nerve endings. It does not synthesize neuropeptides itself, but stores and secrets neuropeptides which were produced in the supraoptic nucleus (SON) and the paraventricular nucleus (PVN) of the hypothalamus. Neurons of the supraoptic nucleus synthesize the prohormone OT-NPI. Neurons of the paraventricular nucleus synthesize the prohormone AVP-NPII. Both prohormones are cleaved into neuropeptides in the axons of neurons which extend into the posterior lobe of the pituitary gland. Cleavage of the prohormone OT-NPI results in a signal peptide, oxytocin and neurophysin I. Cleavage of the prohormone AVP-NPII results in a signal peptide, vasopressin, neurophysin II and copeptin. Details on all neuropeptides discussed in this article (abbreviations, full name, sequence, prohormone from which they are cleaved) are provided in the supporting online material. The intermediate lobe of the pituitary gland consists of epithelial cells and encloses the posterior lobe almost completely. It secretes the neuropeptides γ-MSH, α-MSH, CLIP, γ-LPH and β-endorphin. These neuropeptides are all cleavage products of the prohormone POMC, which is synthesized and cleaved in the intermediate lobe. POMC has eight potential cleavage sites. Processing occurs tissue-dependently and may yield as many as ten biologically active peptides. The anterior lobe is adjacent to the intermediate lobe and is made up of epithelial cells as well. It synthesizes and secretes the neuropeptide ACTH and several (glyco)proteins such as TSH, FSH, LH, GH, PRL.

In this work, we demonstrate that MS imaging of neuropeptides in mammalian tissue is possible at cellular resolution. For the first time such measurements were performed by combining accurate mass analysis, high mass resolving power, MS/MS experiments and high spatial resolution in one instrument.

2. Experimental

2.1. Sample preparation

C57Bl6/N mice (age 12–20 weeks) were decapitated, the pituitary glands were dissected and immediately snap-frozen in liquid nitrogen. Tissue samples were cut in sections of 20 μm thickness with a cryotome (HM500, Microm, Walldorf, Germany) at −20 °C. The sections were thaw-mounted on conductive ITO coated glass slides. The mounted samples were stored at −80 °C until analysis. For measurements, tissue sections were brought to room temperature in a desiccator (30 min) to avoid condensation of humidity on the sample surface. Optical images of tissue sections were taken before sample preparation with an Olympus BX-40 microscope (Olympus Europa GmbH, Hamburg, Germany). No washing steps were applied prior to matrix application. A solution of the matrix 2,5-dihydroxybenzoic acid (DHB; 98% purity, Aldrich, Germany) in a concentrations of 30 mg/mL was prepared in acetone/water (0.1% TFA) 1:1 v/v. The matrix solution was applied with a specially designed pneumatic sprayer [14]. Tissue sections were analyzed immediately after matrix application.

2.2. Instrumentation

All experiments were performed with a home-built atmospheric pressure scanning microprobe matrix assisted laser desorption/ionization imaging source attached to a linear ion trap/Fourier transform orbital trapping mass spectrometer (LTQ Orbitrap Discovery, Thermo Scientific GmbH, Bremen, Germany). The setup of the AP-SMALDI imaging source is given in detail elsewhere [16]. A nitrogen laser (λ = 337 nm, LTB MNL-106, LTB, Berlin, Germany) operating at a repetition rate of 60 Hz was used for desorption/ionization in this study. The laser beam was focused by the centrally bored objective lens to an optical diameter of 8.4 μm ($1/e^2$ definition) [17]. Burn pattern size on tissue (and thus effective sampling size) depended on the applied laser pulse energy (see supplementary online material, Fig. 1) and was adjusted for each experiment to avoid oversampling. Ions from 30 laser pulses were accumulated in the linear ion trap for each mass spectrum. The target voltage was set to 4.3 kV. The step size of the sample stage was set to 5 or 10 μm.

The LTQ Orbitrap instrument was operated in positive-ion mode and in the high mass range mode (m/z = 200–4000). MS imaging measurements were performed using the orbitrap detector with a mass resolving power of 30,000 at m/z = 400. Automatic gain control (AGC) was disabled during the measurement and ion injection time was manually set to 650 ms. External calibration resulted in a

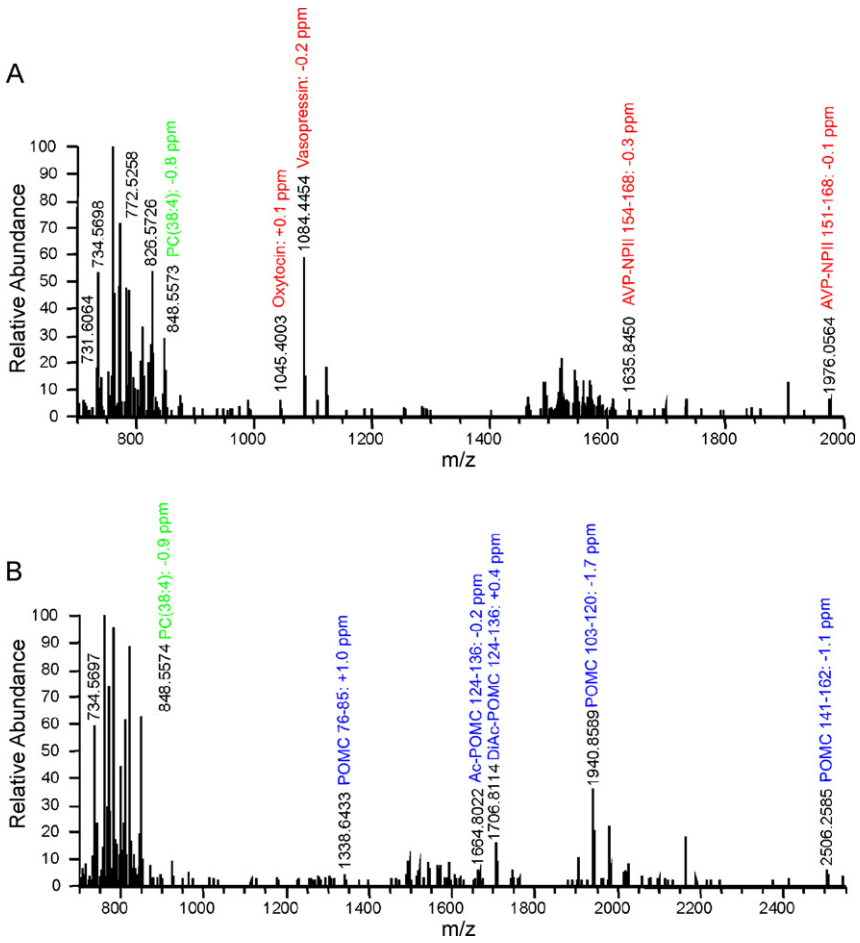

Fig. 2. (A) Single pixel FT mass spectrum from the posterior lobe, (B) single pixel FT mass spectrum from intermediate lobe. Mass accuracy for the peptides was better than 2 ppm. Pixel size was 10 μm.

mass accuracy of <6 ppm under these conditions. A mass accuracy of <2 ppm was achieved by internal calibration using the lock mass feature. The dimer $[2DHB–H_2O+H]^+$, trimer $[3DHB–2H_2O+NH_4]^+$ and pentamer $[5DHB–4H_2O+NH_4]^+$ of DHB as well as the potassium adduct of the phospholipid PC (34:1) were used as lock masses. Cycle times of the ion trap/orbitrap system were 1.3 s (including stage movement).

All MS/MS measurements were performed in the linear ion trap (LTQ) in the normal mass range (m/z = 100–2000) in positive ion mode. Peptide fragmentation was performed via collision induced dissociation (CID). The normalized collision energy was set to a value of 30. The isolation window was $\Delta m/z$ = 3 μm.

2.3. Data processing

2.3.1. Identification of endogenous peptides

A small database of neuropeptides was generated using the data published by Dowell et al. [18], Monroe et al. [19] and Zhang et al. [20]. In addition data listed in the Sweden Peptide Database (www.swepep.org) [21] was added to our database. The Sweden Peptide Database contained 262 entries for the mouse organism in the mass range up to 2000 μm. For all peptides listed in our database, accurate m/z values of the protonated molecular ion $[M+H]^+$, the sodium adduct $[M+Na]^+$, the potassium adduct $[M+K]^+$ and a common matrix adduct $[M+DHB–H_2O+H]^+$ were calculated. A total of 1872 m/z values were used for identification of neuropeptides. During image data evaluation, this list was then compared to a peak list generated from an averaged mass spectrum obtained from the complete imaging measurement by a software tool developed in-house. The peak list of the averaged spectrum contained all peaks having a minimum signal-to-noise level of 2:1 in the mass to charge range 200–4000. A maximum mass deviation of 2 ppm was allowed for the comparison step.

2.3.2. Ion image generation

Generation of selected ion images was performed with the software package MIRION developed in-house. The operation and functionality of the MIRION software will be described in detail elsewhere [22,23]. The imaging software imports raw data files as stored by the LTQ Orbitrap instrument software during image acquisition and connects this mass spectrometric information to additional scanning metadata, stored in separate data files by our ion source control program. This metadata includes the number of lines and columns of the image and the pixel size. Raw data files consist of linear ion trap or FT mass spectra (centroid or profile format). The imaging software is able to create ion images from any of the detected mass-to-charge values with any selected mass accuracy (bin width). A fast image browser of the MIRION software assists selection of images. In this work ion images of selected mass-to-charge values were created from the FT MS data set with a bin width of $\Delta m/z$ = 0.01. Product ion images from MS/MS experiments were created with a bin width of $\Delta m/z$ = 1.0 due to the lower mass resolution and mass accuracy of the linear ion trap. Intensity values in ion images were normalized to the highest intensity measured for each ion species separately. The software, however, allows to normalize to every desirable value. Up to three different ion images

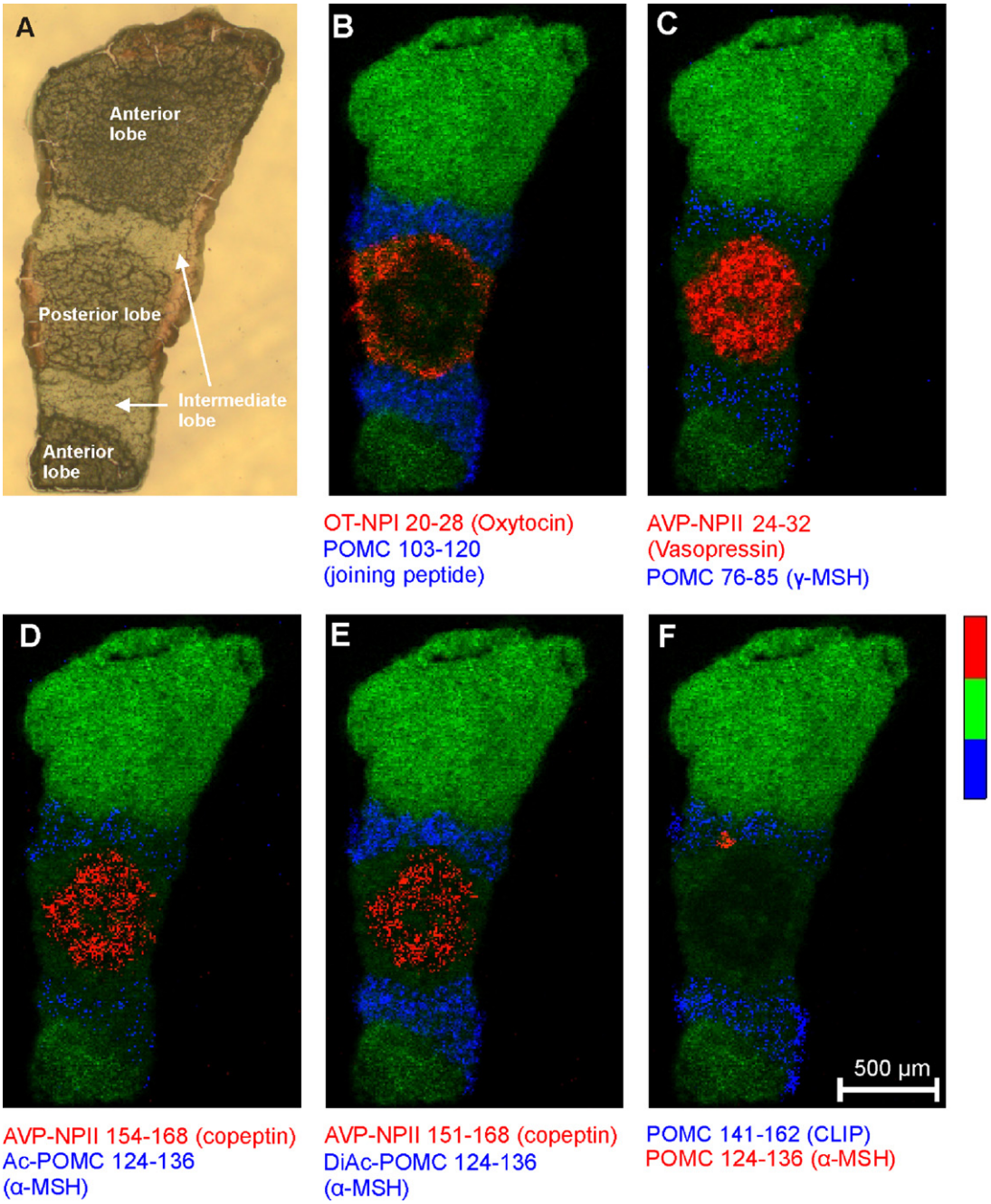

Fig. 3. (A) Optical image of mouse pituitary gland tissue section, (B–F) overlay of selected FT-MS peptide ion images (red + blue) with the ion image of PC (38:4) (green) (bin width: 0.01), 155 × 255 pixels, pixel size was 10 μm.

can be overlayed in RGB images by the software and was used in this work to display up to three ion species in each image. No other postprocessing steps provided by the software (such as interpolation or normalization to matrix signals) were applied to the images, in order to demonstrate the original data quality.

3. Results and discussion

3.1. MS imaging

The MS imaging experiment of mouse pituitary gland was conducted in order to investigate the distribution of neuropeptides within the pituitary gland on a cellular length scale.

An optical image of the measured tissue section is shown in Fig. 3A. Its size was about 1.5 mm (h) × 2.5 mm (v). The posterior lobe is located in the center, while the anterior lobe is located at the bottom and the top of the section. The intermediate lobe is located between anterior lobe and posterior lobe. The whole tissue section was scanned with a step size of 10 μm. Generated ions were detected in the Orbitrap mass analyzer. Fig. 2A shows a typical single pixel FT mass spectrum from the posterior lobe. Fig. 2B shows a typical single pixel FT mass spectrum measured from the intermediate lobe. Mass spectra obtained were of high quality featuring a high number of peaks. A mass accuracy in the low ppm range was obtained and detected intensities varied over the scanned area by about two orders of magnitude. The quality of mass spectra was remarkably good considering that the ions stemed from an area

with a diameter of 8 μm (burn pattern size in this experiment). Most of the peaks in the mass spectra originate from lipids. This was expected, since no washing procedure was applied to the tissue section to remove the lipids. Lipid monomers dominate the mass spectra (m/z = 700–900), but lipid dimers also show a distinct distribution in the mass-to-charge range of 1450–1650. Mass deviation was less than 2 ppm with internal calibration. Mass resolving power in single pixel mass spectra was between 13,000 and 20,000 in the peptide mass range. 10 neuropeptides (Fig. 2, labeled in red and blue) were detected in the mass-to-charge range up to 2500. Due to the specific localization of some peptides, not all peaks were present in the single pixel mass spectra shown in Fig. 2A and B. Peptides were identified by comparing their accurate mass with our database of known neuropeptides. In general the number of matches in database searches strongly depends on the mass tolerance used for identification. The number of false positive matches increases with increasing mass tolerance. Due to the high mass accuracy of the orbitrap mass analyzer the database search could be performed with a mass tolerance of 2 ppm in our study providing for a tentative identification of measured peptides that was subsequently confirmed by MS/MS measurements (see chapter 3.2).

Fig. 3B–F shows the imaged distributions of the identified peptides within the tissue. Each image is an overlay of three individual ion images. The bin size for each ion image was set to $\Delta m/z$ = 0.01. The potassium adduct of the lipid PC (38:4) (colored in green) was used to indicate the overall shape of the pituitary gland. Neuropeptides were colored in red and blue. For comparison Fig. 3A shows the optical image of the tissue section.

The neuropeptides oxytocin and vasopressin were both detected in the posterior lobe (Fig. 3B and C; red), but show different localizations within this tissue. Oxytocin was detected in the outer region of the lobe, while vasopressin was mostly detected in its center. In addition two different fragments of the peptide copeptin were detected in the center of the posterior lobe colocalized with vasopressin (Fig. 3D and E). These results are in excellent agreement with the known anatomical structure of this part of the pituitary gland [24,25]. Oxytocin and vasopressin originate from different prohormons (OT-NPI and AVP-NPII, respectively). These prohormones are synthesized and cleaved in different neurons extending from the supraoptic nucleus (SON) and the paraventricular nucleus (PVN) of the hypothalamus into the posterior lobe. Neurons of the PVN are accumulated in the center of the lobe. Neurons of the SON are mainly located in the outer region. The resulting spatial distribution of vasopressin and oxytocin was clearly resolved in the MS imaging measurements. The same holds for the co-localization of vasopressin and copeptin, both originating from the same prohormone (AVP-NPII).

The neuropeptide α-MSH was detected in the intermediate lobe in its unmodified (Fig. 3F, red) and two modified forms: the acetylated and diacetylated (Fig. 3D and E, blue). These results correspond well with the literature [26]. α-MSH is the main neuropeptide secreted by the intermediate lobe. In adult mice it is acetylated before it is secreted resulting in increased stability and bioactivity. While the acetylated and the diacetylated α-MSH is homogeneously distributed in the intermediate lobe, the unmodified α-MSH is only detected in a very small area. The unmodified α-MSH detected in this tissue section was therefore most likely due to newly generated peptides that were not acetylated yet.

Three other peptides γ-MSH (Fig. 3C, blue), joining peptide (Fig. 3B, blue) and CLIP (Fig. 3F, blue) were also detected in this part of the pituitary gland. All these peptides are cleavage products of the same prohormone POMC, which is synthesized and cleaved in the intermediate lobe. No peptides were detected in the anterior lobe as most hormones secreted in this part of the gland are (glyco)proteins and are therefore beyond the detected mass range.

All detected peptide distributions were found to be in good agreement with the physiological structure and biological function of the pituitary gland. Ion images of the peptides allow a clear assignment of the three different lobes as well as further differentiation within these tissues. In addition to high spatial resolution these images are highly specific since they are generated from high resolution mass spectral data. The orbitrap mass analyzer is able to resolve the complex composition of the biological tissue sample with high reproducibility over the measurement period. The (small) imaging bin width of $\Delta m/z$ = 0.01 ensures that the displayed intensity distribution only represents one single peptide/compound and is not affected by neighboring peaks.

Results presented here are only semi-quantitative in nature. Signal intensities in mass spectra are not directly correlated to peptide concentrations in tissue but are influenced by additional parameters such as physico-chemical properties of the analytes and of the surrounding tissue matrix as a local environment. Substances may compete for ionization in a complex mixture and may suppress ionization of unfavored species. Ionization efficiencies are typically rather constant within a given tissue type, but are often strongly differing between different tissue types [27]. A systematic determination of tissue-dependent sensitivity factors and subsequent signal intensity correction was beyond the scope of this study but have to be considered for a quantitative study of neuropeptides in tissue in the future. Until today, quantitatively corrected MS imaging has only very rarely been reported.

3.2. Peptide verification by MS/MS

Accurate assignment of a signal in the mass spectrum to a specific substance is one of the key issues in mass spectrometry. This is especially true for complex samples such as biological tissue. The application of accurate mass measurements used in this study significantly improves the reliability of compound identification by reducing the number of candidate peptides. Mass peaks in this study were tentatively identified by a targeted database search of known neuropeptides. In order to verify these assignments we performed additional MS/MS experiments.

These measurements were performed directly on tissue at high spatial resolution (pixel size: 10 μm). Precursor ions where fragmented via collision induced dissociation (CID) and product ions were analyzed in the linear ion trap due to the lower limit of detection (LOD) of this mass analyzer. Fig. 4 shows averaged MS/MS spectra of selected precursor ions. Each MS/MS spectrum features a number of product ions which give additional information on the peptide sequence. All tentative identifications of neuropeptides could be confirmed with this method. The possibility to perform MS/MS measurements directly from tissue allows fast and reliable verification of substance identification. In the past, MS/MS verification of imaged compounds was often not possible directly from tissue due to sensitivity problems, and identification had to be performed by separate bulk experiments usually involving sample homogenization and chromatographic separation. This approach is much more laborious and time-consuming and also holds a high risk for misassignments and artifacts.

3.3. MS/MS imaging

Even if the neuropeptides were identified by accurate mass measurements and the identification was confirmed by on-tissue MS/MS measurements, there is still the possibility for a false assignment by an arbitrary co-localization of isobaric compounds. MS/MS measurements shown in chapter 3.2 were performed on a limited area only. In order to confirm the validity of this approach a larger area including all three lobes of the pituitary gland was imaged in MS/MS mode. An identical image distribution of precursor and

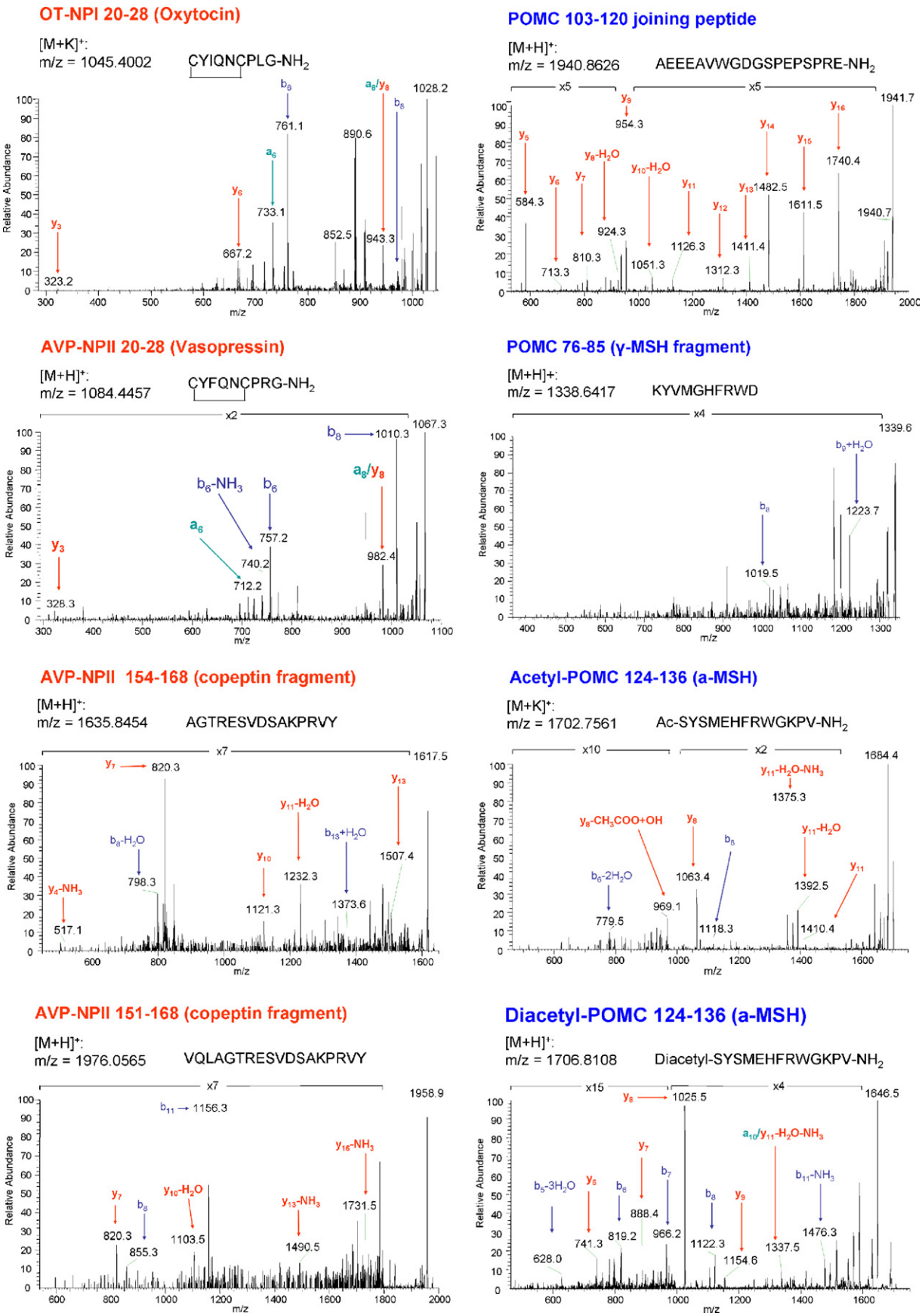

Fig. 4. Identification of neuropeptides via MS/MS: (left column) peptides present in the posterior lobe, (right column) peptides present in the intermediate lobe. Each MS/MS spectrum features a high number of product ions confirming the identity of the assumed peptide.

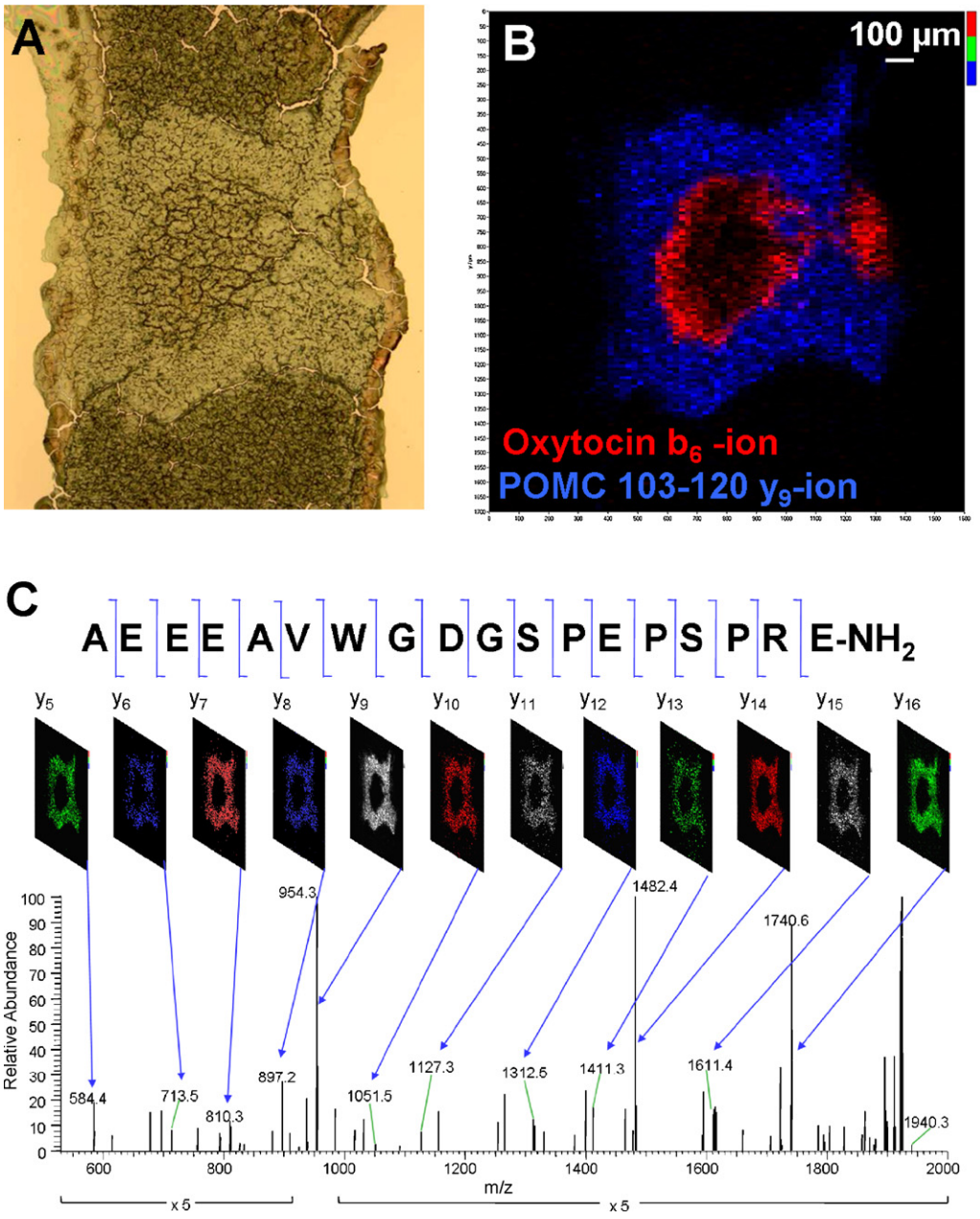

Fig. 5. MS/MS imaging of neuropeptides in mouse pituitary gland: (A) optical image of the tissue section (B) overlay of selected IT-MS/MS peptide product ion images (bin width: $\Delta m/z = 1$), 160 × 170 pixels, pixel size was 20 μm × 10 μm, (C) single pixel IT MS/MS spectrum of the precursor ion assigned to the peptide POMC 103–120 ($m/z = 1940.8626$). Almost the complete y-ion series of the peptide POMC 103–120 was detected and imaged. All product ion images show the same distribution, as expected for a valid signal assignment.

product ion was expected for a valid product ion assignment. Two peptide precursor ions were selected to be analyzed on another tissue section. Fig. 5A shows the optical image of the measured area of the pituitary tissue section. The anterior lobe is located at the bottom and at the top of the optical image. The posterior lobe is located in the center. The intermediate lobe is located between anterior lobe and posterior lobe. The experiment was performed with the same spatial resolution as the MS imaging measurement (pixel size: 10 μm). Two precursor ions corresponding to the peptides oxytocin and POMC 103–120 were alternately fragmented. Precursor ions were fragmented by CID and product ions were analyzed in the linear ion trap due to its higher duty cycle compared to the orbitrap analyzer. Since each precursor ion was fragmented from a fresh sample spot, the resulting pixel size was 20 μm × 10 μm for each product ion image. Fig. 5B shows an overlay of two product ion images. The b_6 product ion of oxytocin was colored in red and the y_9 product ion of POMC 103–120 was colored in blue in this image. These ion images correspond very well to the distribution of the corresponding precursors in the MS imaging experiment (Fig. 2).

The fact that the product ion images are of similar quality as the precursor ion image shows the reliability and sensitivity of the MS/MS method of our instrumental setup. It is not limited to certain areas of high concentration but is achieved over the whole measurement area. This is demonstrated in Fig. 5C for the peptide precursor POMC 103–120. Product ions corresponding to almost the complete y-ion series of the peptide were detected in single-pixel IT MS/MS spectra. Product ion images were generated for each y-ion. All of these images resemble the distribution of the precursor peptide in the gland with excellent quality. The high number of product ion peaks from single-pixel MS/MS spectra could be used

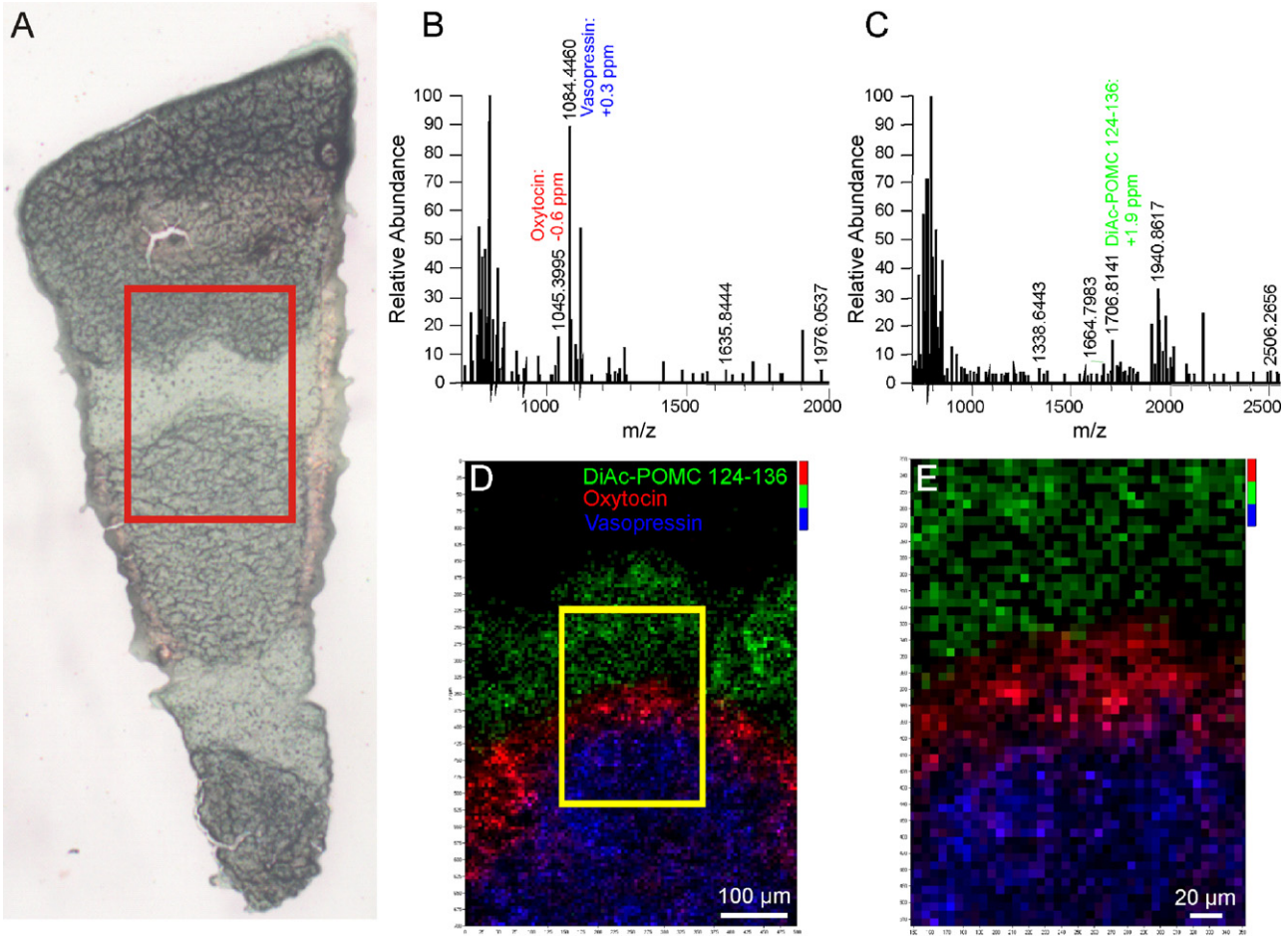

Fig. 6. (A) Optical image of mouse pituitary tissue section. The region measured in the MS imaging experiment is indicated by a red square. (B) Single-pixel FT mass spectrum from the posterior lobe. (C) Single-pixel FT mass spectrum from the intermediate lobe (mass accuracy for the peptides was ≤2 ppm), (D) Overlay of selected peptide ion images (bin width: $\Delta m/z = 0.01$), 100 × 140 pixels. Pixel size was 5 μm. The peptide diacetyl-α-MSH was located in the intermediate lobe (green), the peptides oxytocin (red) and vasopressin (blue) are located in the posterior lobe. (E) Enlarged view of the border between intermediate and posterior lobe as indicated in (D) by a yellow square.

for de novo sequencing of unknown peptides in other experiments. MS/MS analysis is also helpful when identifying endogenous peptides via an untargeted database search. Neuropeptide precursors are cleaved specifically by following individual rules and are subject to post-translational modification. Neuropeptides are therefore rather difficult to identify with untargeted ('no enzyme') database searches. Each additional information thus reduces the number of peptide candidates.

By imaging of product ions both, the identity of precursor ions and their distribution was confirmed. This confirmation is even more important when mass spectrometers featuring a low mass accuracy and mass resolving power, such as the linear ion trap are used for MS imaging. By including product ion images, a high selectivity and reliability can be obtained even without accurate mass. Here we showed that this is even possible at a high spatial resolution.

3.4. MS imaging of peptides at 5 μm spatial resolution

In order to investigate the fine structure of the pituitary gland in more detail we conducted an MS imaging experiment on another tissue section with a spatial resolution of 5 μm. Fig. 6A shows the optical image of the tissue section. The red rectangle indicates the measured area that includes the anterior lobe (top), intermediate lobe (center) and posterior lobe (bottom). Fig. 6B and C show single-pixel FT mass spectra from the posterior and intermediate lobe, respectively. Mass spectra are still of high quality, although the reduction of the pixel size resulted in a decrease of the total ion current to about 50%. Nevertheless 9 of the 10 peptides identified in the 10 μm MS imaging experiment were also detected at 5 μm resolution. Only the unmodified α-MSH was not detected from this tissue section, probably due to its apparently highly specific localization in individual sections (Fig. 2F). Signals of the peptides were labeled with their mass-to-charge ratio in the mass spectra. A mass deviation of less than 2 ppm was achieved in this experiment after internal calibration. Fig. 6D shows an overlay of selected peptide ion images. Oxytocin is displayed in red, vasopressin is colored in blue and diacetyl-α-MSH is colored in green. Localization of these neuropeptides is in good agreement to that shown in Fig. 3. Vasopressin was detected in the center of the posterior lobe. Oxytocin was detected in the outer part of the posterior lobe and diacetyl-α-MSH was detected in the intermediate lobe.

Fig. 6E shows an enlarged view of the border between different tissue types (marked by a yellow square in Fig. 6D). It is apparent from this enlarged view that diacetyl-α-MSH (green) is not homogeneously distributed in the intermediate lobe but expresses a fine structure, indicated by a large number of black pixels adjacent to areas of intense signals shown in green. This observation corresponds well to the known cellular structure of this lobe. The intermediate lobe consists of epithelial cells being 10–20 μm in size and being composed of two subtypes: basophilic and chromophobeic cells. Only the basophilic cells produce α-MSH. The green pixels therefore are assumed to indicate basophilic cells while the black pixels should indicate chromophobeic cells not producing α-

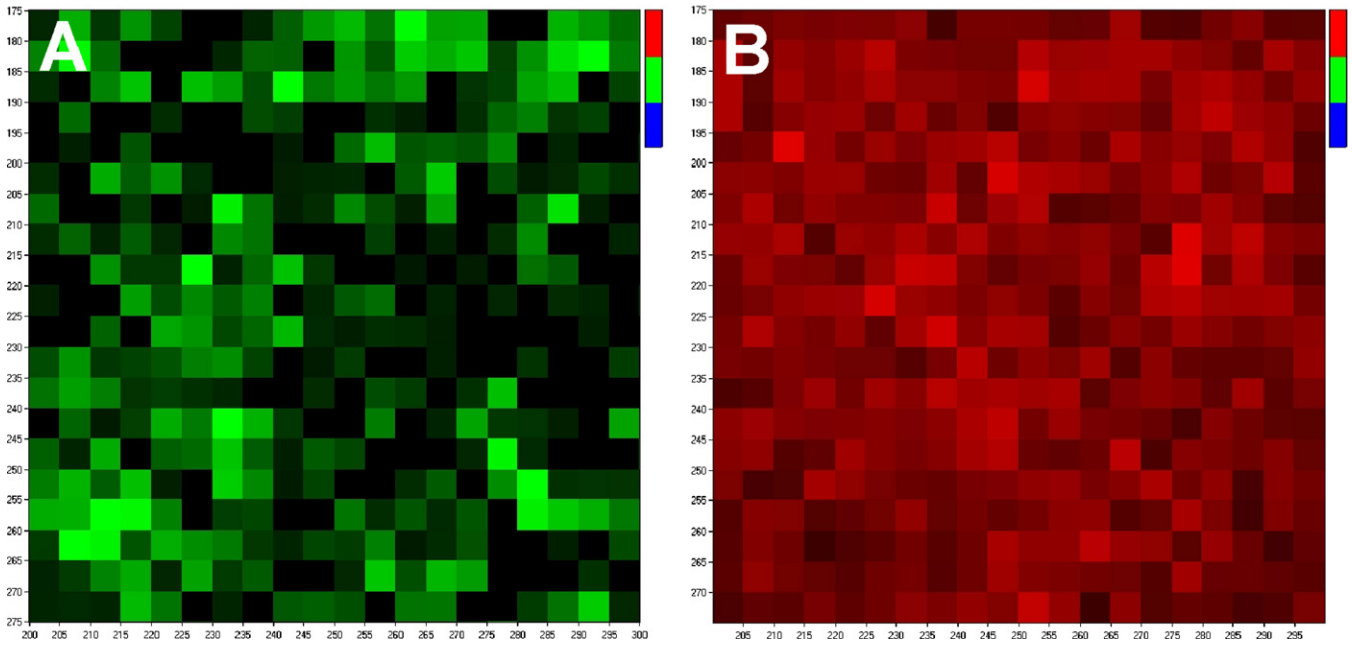

Fig. 7. (A) Selected ion image of diacetyl-α-MSH in the pituitary intermediate lobe, enlarged view (100 μm × 100 μm) of Fig. 6D. (B) Selected ion image of the potassium adduct of the phospholipid PC (32:0) in the same region of the intermediate lobe.

MSH. This shows that our MS imaging experiment at 5 μm pixel size allows us to differentiate tissue types on a cellular level.

Black pixels (missing signal intensities) were confirmed to be not due to preparational artifacts as other compounds are detected at these positions. To demonstrate this, Fig. 7 shows the distribution of diacetyl-α-MSH in the intermediate lobe in comparison to the distribution of the phospholipid PC (32:0) in the same area. While diacetyl-α-MSH features an inhomogeneous, well-structured distribution, the phospholipid is homogenously distributed over the whole area indicating a uniform ion formation activity over the imaged sample area. Also black pixels were found to be not a result of inhomogeneous ion suppression effects. Ion suppression is a common phenomenon due to interaction of different compounds during ion formation. It is known to vary with the analyte's local environment as present in a certain tissue type. Ion suppression is on the other hand expected to be rather constant within a given tissue environment. In a high-resolution imaging experiment, the small laser focus will evaporate material from only one tissue type and ion suppression will not be influenced by compounds from neighboring tissue types as with larger laser foci. Compared to the 10 μm imaging experiment in Fig. 3, ion intensity artifacts caused by ion suppression effects can thus only be less pronounced in the 5 μm imaging experiment shown in Fig. 6.

Fig. 6E also shows the borderline between the intermediate lobe and the posterior lobe. There is almost no signal overlap between the distribution of α-MSH (green) and oxytocin (red) indicating a sharp border between the two tissue types. Pixels at the borderline are either colored green or red. Only a few pixels are colored yellow (=green + red), which would indicate that both oxytocin and α-MSH are present in the mass spectrum of the same pixel. This corresponds well to the anatomical fact that intermediate lobe and posterior lobe are separated by a sharp border (with no mixing of cells from the two tissues) [28].

In contrast the border between vasopressin (red) and oxytocin (blue) within the posterior lobe is less well defined (Fig. 6E). A clear overlap of the distribution of these two neuropeptides is observed. At the borderline several pixels are colored in magenta (=red + blue), which shows that oxytocin and vasopressin were detected in the same pixel. The posterior lobe consists mainly of nerve endings which have a maximum size of 5 μm. Nerve endings of neurons extending from the PVN into this lobe contain vasopressin and are accumulated in the center. Nerve endings of neurons extending from the PVN contain oxytocin and are accumulate in its outer regions. The border between these different nerve endings is not well defined. There is a region where both nerve ending types are mixed [28]. The size of these cells is in the same range as the laser focus and therefore the two cell types cannot be completely differentiated. This results in magenta pixels at the border between the two neuropeptide distributions.

These results show that the fine structure of the pituitary gland can be resolved by our method on a cellular level. The fact that the sharp border between intermediate lobe and posterior lobe is resembled correctly in the ion image also shows the quality of our matrix preparation. The spatial integrity of the analytes was preserved within the size of one pixel during the sample preparation. No further diffusion of the analytes was caused by wetting of the sample. The size of matrix crystals was smaller or equal to the raster step size of 5 μm (supplementary Fig. 2). A diffusion of the analytes by wetting of the sample would result in a stronger overlap of peptide distributions. The number of yellow pixels at the borderline between the intermediate lobe and posterior lobe in this case would be higher than observed in this experiment.

4. Conclusions

In this work, we combined high spatial resolution, high mass resolving power, high mass accuracy and MS/MS capabilities under atmospheric pressure conditions in one instrument for MALDI imaging of tissue. We present the first MS images of neuropeptides at 5 μm effective spatial resolution obtained in the microprobe imaging mode and without considerable oversampling. A similar spatial resolution was reported in the so-called microscope imaging mode [6] where ions were selected by a ion blanker and only one *m/z* bin was detected per experiment. In contrast our measurements result in mass spectral data for the full analyzed mass range simultaneously. Previous microprobe imaging studies of neuropeptides had reported a spatial resolution of 30–250 μm [9,29,30]. Due to the lower spatial resolution of these measurements, borders of

the tissue and between tissue types were blurred and neuropeptide distributions were shown in much less detail. Our MS measurements show distinct physiological features and have high pixel coverage due to a homogenous matrix application. This resulted in MS images of high quality without the need for pixel interpolation or other postprocessing steps.

Analytes in our MS imaging experiments were detected with accurate mass and high mass resolving power allowing for confident compound identification and highly specific image generation. Imaging measurements performed with high mass accuracy and high mass resolving power were presented previously [7,8], but they did not feature high spatial resolution at the same time. The same is true for identification/verification of neuropeptide via MS/MS measurements [10,11] on tissue and MS/MS imaging [8] of neuropeptide product ions.

Acknowledgements

Financial support by the State of Hesse (LOEWE Research Focus 'Ambiprobe'), by the European Union (STREP project LSHG-CT-2005-518194) and by the Bundesministerium für Bildung und Forschung (BMBF, NGFN project 0313442) is gratefully acknowledged. We thank Tamara Papadakis for preparing the cryosections and Zoltan Takats for letting us use the orbitrap (European Research Council Starting Grant 2008). This publication represents a component of the doctoral (Dr. rer. nat.) thesis of S.G. at the Faculty of Biology and Chemistry, Justus Liebig University Giessen, Germany.

Appendix A. Supplementary data

Supplementary data associated with this article can be found, in the online version, at doi:10.1016/j.ijms.2010.11.011.

References

[1] A.F.M. Altelaar, I.M. Taban, L.A. McDonnell, P.D.E.M. Verhaert, R.P.J. de Lange, R.A.H. Adan, W.J. Mooi, R.M.A. Heeren, S.R. Piersma, High-resolution MALDI imaging mass spectrometry allows localization of peptide distributions at cellular length scales in pituitary tissue sections, International Journal of Mass Spectrometry 260 (2–3) (2007) 203–211.
[2] R.J.A. Goodwin, S.R. Pennington, A.R. Pitt, Protein and peptides in pictures: imaging with MALDI mass spectrometry, Proteomics 8 (18) (2008) 3785–3800.
[3] A.B. Hummon, A. Amare, J.V. Sweedler, Discovering new invertebrate neuropeptides using mass spectrometry, Mass Spectrometry Reviews 25 (1) (2006) 77–98.
[4] B. Spengler, M. Hubert, Scanning microprobe matrix-assisted laser desorption ionization (SMALDI) mass spectrometry: instrumentation for sub-micrometer resolved LDI and MALDI surface analysis, Journal of the American Society for Mass Spectrometry 13 (6) (2002) 735–748.
[5] M. Stoeckli, P. Chaurand, D.E. Hallahan, R.M. Caprioli, Imaging mass spectrometry: a new technology for the analysis of protein expression in mammalian tissues, Nature Medicine 7 (4) (2001) 493–496.
[6] A.F.M. Altelaar, I. Klinkert, K. Jalink, R.P.J. de Lange, R.A.H. Adan, R.M.A. Heeren, et al., Gold-enhanced biomolecular surface imaging of cells and tissue by SIMS and MALDI mass spectrometry, Analytical Chemistry 78 (3) (2006) 734–742.
[7] I.M. Taban, A.F.M. Altelaar, Y.E.M. Van der Burgt, L.A. McDonnell, R.M.A. Heeren, J. Fuchser, et al., Imaging of peptides in the rat brain using MALDI-FTICR mass spectrometry, Journal of the American Society for Mass Spectrometry 18 (1) (2007) 145–151.
[8] R.B. Chen, X.Y. Jiang, M.C.P. Conaway, I. Mohtashemi, L.M. Hui, R. Viner, et al., Mass spectral analysis of neuropeptide expression and distribution in the nervous system of the Lobster Homarus americanus, Journal of Proteome Research 9 (2) (2010) 818–832.
[9] R.B. Chen, L.M. Hui, R.M. Sturm, L.J. Li, Three dimensional mapping of neuropeptides and lipids in crustacean brain by mass spectral imaging, Journal of the American Society for Mass Spectrometry 20 (6) (2009) 1068–1077.
[10] S.S. DeKeyser, K.K. Kutz-Naber, J.J. Schmidt, G.A. Barrett-Wilt, L.J. Li, Imaging mass spectrometry of neuropeptides in decapod crustacean neuronal tissues, Journal of Proteome Research 6 (5) (2007) 1782–1791.
[11] P.D. Verhaert, M.C.P. Conaway, T.M. Pekar, K. Miller, Neuropeptide imaging on an LTQ with vMALDI source: the complete 'all-in-one' peptidome analysis, International Journal of Mass Spectrometry 260 (2–3) (2007) 177–184.
[12] A. Römpp, S. Guenther, Y. Schober, O. Schulz, Z. Takats, W. Kummer, et al., Histology by mass spectrometry: label-free tissue characterization obtained from high-accuracy bioanalytical imaging, Angewandte Chemie-International Edition 49 (22) (2010) 3834–3838.
[13] P. Chaurand, R.M. Caprioli, Direct profiling and imaging of peptides and proteins from mammalian cells and tissue sections by mass spectrometry, Electrophoresis 23 (18) (2002) 3125–3135.
[14] W. Bouschen, O. Schulz, D. Eikel, B. Spengler, Matrix vapor deposition/recrystallization and dedicated spray preparation for high-resolution scanning microprobe matrix-assisted laser desorption/ionization imaging mass spectrometry (SMALDI-MS) of tissue and single cells, Rapid Communication in Mass Spectrometry 24 (3) (2010) 355–364.
[15] M. Kaufman, A.Y. Nikitin, J.P. Sundberg, Histologic basis of mouse endocrine system development: a comparative analysis, CRC Press Taylor & Francis Group, 2010.
[16] M. Koestler, D. Kirsch, A. Hester, A. Leisner, S. Guenther, B. Spengler, A high-resolution scanning microprobe matrix-assisted laser desorption/ionization ion source for imaging analysis on an ion trap/Fourier transform ion cyclotron resonance mass spectrometer, Rapid Communications in Mass Spectrometry 22 (20) (2008) 3275–3285.
[17] S. Guenther, M. Koestler, O. Schulz, B. Spengler, Laser spot size and laser power dependence of ion formation in high resolution MALDI imaging, International Journal of Mass Spectrometry 294 (1) (2010) 7–15.
[18] J.A. Dowell, W. Vander Heyden, L. Li, Rat neuropeptidomics by LC–MS/MS and MALDI-FTMS: enhanced dissection and extraction techniques coupled with 2D RP-RP HPLC, Journal of Proteome Research 5 (12) (2006) 3368–3375.
[19] E.B. Monroe, S.R. Annangudi, N.G. Hatcher, H.B. Gutstein, S.S. Rubakhin, J.V. Sweedler, SIMS and MALDI MS imaging of the spinal cord, Proteomics 8 (18) (2008) 3746–3754.
[20] X. Zhang, F.Y. Che, I. Berezniuk, K. Sonmez, L. Toll, L.D. Fricker, Peptidomics of Cpe(fat/fat) mouse brain regions: implications for neuropeptide processing, Journal of Neurochemistry 107 (6) (2008) 1596–1613.
[21] M. Fälth, K. Sköld, M. Norrman, M. Svensson, D. Fenyö, P.E. Andren, SwePep, a database designed for endogenous peptides and mass spectrometry, Molecular and Cellular Proteomics 5 (6) (2006) 998–1005.
[22] A. Hester, W. Bouschen, A. Leisner, K. Maass, C. Paschke, B. Spengler, 53rd ASMS Conference on Mass Spectrometry and Allied Topics, San Antonio, Texas, USA; June 5–9, 2005.
[23] Paschke C, Leisner A, Hester A, Maass K, Bouschen W, Spengler B. in preparation.
[24] F.W. van Leeuwen, C. Deraay, D.F. Swaab, B. Fisser, Localization of oxytocin, vasopressin, somatostatin and luteinizing hormone releasing hormone in the rat neurohypophysis, Cell and Tissue Research 202 (2) (1979) 189–201.
[25] B.J. Zhang, K. Kusano, P. Zerfas, A. Iacangelo, W.S. Young, H. Gainer, Targeting of green fluorescent protein to secretory granules in oxytocin magnocellular neurons and its secretion from neurohypophysial nerve terminals in transgenic mice, Endocrinology 143 (3) (2002) 1036–1046.
[26] D. Rudman, B.M. Hollins, M.H. Kutner, S.D. Moffitt, M.J. Lynn, Three types of alpha-melanocyte-stimulating hormone – bioactivities and half-lives, American Journal of Physiology 245 (1) (1983) E47–E54.
[27] M. Stoeckli, D. Staab, A. Schweitzer, Compound and metabolite distribution measured by MALDI mass spectrometric imaging in whole-body tissue sections, International Journal of Mass Spectrometry 260 (2–3) (2007) 195–202.
[28] S. Schimchowitsch, M.E. Stoeckel, M.J. Klein, J.C. Garaud, G. Schmitt, A. Porte, Oxytocin-immunoreactive nerve fibers in the pars intermedia of the pituitary in the rabbit and hare, Cell and Tissue Research 228 (2) (1983) 255–263.
[29] M.R. Groseclose, M. Andersson, W.M. Hardesty, R.M. Caprioli, Identification of proteins directly from tissue: in situ tryptic digestions coupled with imaging mass spectrometry, Journal of Mass Spectrometry 42 (2) (2007) 254–262.
[30] P. Chaurand, S. Fouchecourt, B.B. DaGue, B.G.J. Xu, M.L. Reyzer, M.C. Orgebin-Crist, et al., Profiling and imaging proteins in the mouse epididymis by imaging mass spectrometry, Proteomics 3 (11) (2003) 2221–2239.